


Proton heating estimates from near-Earth observations of coronal mass ejections in solar cycle 24

Debesh Bhattacharjee¹ ,¹★ Prasad Subramanian,² Saikat Majumder³ and Wageesh Mishra⁴

¹*School of Physics and Astronomy, Kelvin Building, University of Glasgow, University Avenue, Glasgow G12 8QQ, UK*

²*Department of Physics, Indian Institute of Science Education and Research Pune, Dr Homi Bhabha Road, Pashan, Pune 411008, Maharashtra, India*

³*Astrodynamics Team, Digantara Research and Technologies Pvt. Ltd., Floor 9, Brigade Senate 2, Hebbal Kempapura-560024, Bengaluru, Karnataka, India*

⁴*Department of Sun and Solar System, Indian Institute of Astrophysics, 100 Feet Rd, Santhosapuram, 2nd Block, Koramangala, Bengaluru 560034, Karnataka, India*

Accepted 2025 May 19. Received 2025 April 11; in original form 2024 November 15

ABSTRACT

As solar coronal mass ejections (CMEs) propagate through the heliosphere, they expend energy in heating protons to compensate for the cooling that occurs due to expansion. CME propagation models usually treat energy dissipation implicitly via a polytropic index (δ). Here, we calculate the power dissipation implied by a given δ and compare it with the power available in the turbulent velocity fluctuations. We make this comparison using near-Earth *in situ* observations of 27 of the most geoeffective CMEs ($D_{\text{st}} < -75$ nT) in solar cycle 24. For $\delta = 5/3$, the power in the turbulent velocity fluctuations is ≈ 54 per cent smaller than what would be required to maintain the proton temperature at the observed values. If the power in the turbulent cascade is assumed to be fully expended in local proton heating, the most probable value for δ is 1.35. Our results contribute to a better understanding of CME energetics, and thereby to improved CME propagation models and estimates of Earth arrival times.

Key words: turbulence – methods: data analysis – Sun: coronal mass ejections (CMEs).

1 INTRODUCTION

Solar coronal mass ejections (CMEs) aimed at the Earth are some of the primary drivers of space weather disturbances. It is therefore no surprise that predictions of CME arrival times and speeds at the Earth constitute one of the most active fields of research in heliophysics (Gopalswamy et al. 2001; Riley et al. 2018). Models of CME propagation through the heliosphere use observations of near-Sun CME launch times and speeds to predict when they will arrive at the Earth. The energy contained in the CME magnetic fields is usually considered to be the primary reservoir (Mandrini 2010), which is expended in (i) driving the CME through the heliosphere, overcoming losses due to aerodynamic drag with the ambient solar wind and (ii) in compensating for the cooling of the CME plasma as it expands outwards. Unfortunately, the relative importance of these processes is not very well known. Consequently, basic model parameters need to be tuned in order to obtain approximate agreement with CME Earth arrival times. In this paper, we focus on item (ii) – local heating of the CME plasma (technically, only the protons) as it propagates and expands outwards. It is well known that the CME plasma is subjected to local heating as it propagates outwards. This is borne out, for instance, by UVCS observations at $\approx 2.4R_{\odot}$ (Akmal et al. 2001; Ciaravella et al. 2001; Lee et al. 2009; Murphy, Raymond & Korreck 2011). CME propagation models typically use a one-fluid description, with no distinction between the constituents of

the CME plasma, such as protons, electrons, and other heavier ions. The term ‘plasma heating’ is taken to mean heating of the entire (one-fluid) plasma. Such models use a polytropic law ($P V^{\delta} = \text{Constant}$) to implicitly address the CME plasma heating rate. An isothermal process ($\delta = 1$) suggests that the gas is connected with an external heat reservoir, so that there is constant heat supply, enabling it to maintain its temperature. On the other hand, for an adiabatic process ($\delta = 5/3$), the gas is thermally isolated from its surroundings and its internal energy changes in response to the work expended in compressing or expanding the gas. Values of $\delta \approx 1$ imply that the plasma is nearly isothermal, so that the temperature is maintained at a nearly constant value owing to continuous heat transfer from the hot solar corona, without need for local heating. Conversely, $\delta \approx 5/3$ implies that the CME plasma is nearly adiabatic (i.e. there is no external heat supply), which would demand a relatively large local heating rate to compensate for the cooling of the CME as it expands. There is no consensus on the ‘correct’ value of δ to use, either in one-dimensional CME propagation models (Chen 1996; Kumar & Rust 1996) or in 3D MHD simulations (Odstrčil & Pizzo 1999; Lionello et al. 2013; Pomoell & Poedts 2018; Odstrčil 2023).

Several authors use scatterplots between density and temperature from *in situ* observations to calculate the polytropic index of protons. Totten, Freeman & Arya (1995) and Nicolaou et al. (2020) use this technique for the proton polytropic index in the solar wind. Osheerovitch et al. (1993) studied the thermodynamics inside interplanetary CMEs (ICMEs) using density–temperature scatterplots. They found that the proton polytropic index inside ICMEs is ≈ 1.2 and electron polytropic index is ≈ 0.48 . Dayeh & Livadiotis (2022) used

* E-mail: debesh.bhattacharjee@glasgow.ac.uk

density–temperature scatterplots for a set of 336 events to determine the polytropic index inside ICMEs, sheath, and the pre- and post-event regions. They found that inside ICMEs, the polytropic index is ≈ 0.13 lower than the adiabatic value ($5/3$). Farrugia, Osherovich & Burlaga (1995) found that self-similar radially expanding magnetic flux tube solutions for ICMEs require a polytropic index < 1 , while spheromak solutions require it to be $4/3$. Using ICME observations between 0.3 and 5.4 au, Liu, Richardson & Belcher (2005) found that the proton polytropic index in ICME protons is ≈ 1.15 and the electron polytropic index is ≈ 0.73 .

Wang, Zhang & Shen (2009), Mishra & Wang (2018), and Khuntia et al. (2023) use the observed self-similar expansion of CMEs together with an assumption of self-similarity for the proton polytropic index to surmise that it varies from $\approx 5/3$ near the Sun to ≈ 1.2 near the Earth. In this paper, we use the polytropic index as a free parameter and explicitly compute the predicted CME proton heating rate. We compare this prediction with the power available in the turbulent velocity fluctuation spectrum that can potentially heat the protons.

The rest of the paper is organized as follows: Section 2 describes the polytropic model for the temperature evolution of CME protons. We also mention the formula for the power available in the turbulent velocity spectrum in Section 3. Section 4 and Section 5 describe the data we use and the results obtained in this study, respectively. Section 6 contains discussion and conclusions.

2 HEATING RATE PREDICTED BY A POLYTROPIC PROCESS

In this section we outline the procedure to estimate the power required to compensate for cooling of protons as a CME expands. We assume that the CME plasma follows a polytropic law

$$PV^\delta = \text{Constant}, \quad (1)$$

where P , V , and δ are the pressure, volume, and the polytropic index, respectively. We follow well-established treatments of energy conservation processes in the solar wind and obtain an expression for the local energy dissipation rate corresponding to a given value of δ . The details are mentioned in Appendix A2, and we quote the main result here, which concerns the evolution of proton temperature T :

$$\frac{dT(R)}{dR} = 84.32(\gamma - 1) \frac{\epsilon(R)}{U(R)} - 3(\delta - 1) \frac{T(R)}{R}, \quad (2)$$

where R is the heliocentric distance in units of solar radii (so that $R = 215$ at the Earth), $U(R)$ is the CME velocity in units of km s^{-1} , ϵ is the local plasma heating rate inside the CME in $\text{J kg}^{-1} \text{s}^{-1}$, $\gamma \equiv C_p/C_v$ is the adiabatic index, and δ is the polytropic index. The first term on the right-hand side involving ϵ represents ‘additional’ local heating due to an unspecified source. It can be due to small-scale reconnection inside the CME plasma, or due to dissipation of energy contained in turbulent fluctuations. Equation (2) is similar to equation (9) of Vasquez et al. (2007), except that (i) it does not presume that the CME plasma expands adiabatically; δ can take on any value, including $\gamma \equiv C_p/C_v$, and (ii) the CME is assumed to expand in a self-similar manner during its propagation, so that (as explained in Appendix A2) $V \propto R^3$. Several observational studies show that CMEs expand self-similarly, at least beyond $\approx 10 R_\odot$. Subramanian et al. (2014) studied a well-observed sample of CMEs in the field of view of the Sun–Earth Connection Coronal and Heliospheric Investigation coronagraphs onboard the Solar Terrestrial Relationship Observatory (STEREO) satellite using the graduated cylindrical shell model (Thernisien 2011) and found that CMEs propagate self-

similarly as they propagate through the solar wind. A recent study of 475 CMEs observed by the STEREO satellite reveals that the ratio between the CME propagation speed and lateral expansion speed is constant, implying self-similar expansion (Balmaceda et al. 2020). Möstl & Davies (2013) use the analytical Self-Similar Expansion Fitting model (Davies et al. 2012) to estimate CME arrival speeds and times at the Earth. Wang et al. (2009) investigate the thermodynamics of CMEs by determining the heliocentric evolution of polytropic index, Lorentz force, and gas pressure force under the assumption of self-similar expansion of CMEs.

With no additional local energy deposition inside the CME ($\epsilon = 0$), and adiabatic expansion ($\delta = \gamma$, i.e. no connection to an external heat reservoir), equation (2) predicts that a CME with a proton temperature of 10^6 K at $1.05 R_\odot$ will cool to $\approx 24 \text{ K}$ when it reaches the Earth. This highlights the need for additional local energy deposition (i.e. $\epsilon \neq 0$) to account for the observed temperatures of $\approx 10^5 \text{ K}$ at 1 au, if the CME is assumed to expand adiabatically. On the other hand, if $\epsilon = 0$ (no local heating) and the plasma is isothermal (i.e. $\delta = 1$ and it is implied that the CME plasma is connected to an external energy reservoir such as the solar corona), equation (2) predicts that the proton temperature remains unchanged, as expected.

As with most solar wind models, we assume that the proton temperature in the CME varies as a power law with the heliocentric distance as assumed in Démoulin (2009) and references therein.

$$T = T_0 \left(\frac{R}{R_0} \right)^{-\alpha}, \quad (3)$$

where T_0 is the proton temperature at a reference heliocentric distance R_0 . Using equation (3), the temperature evolution equation (equation 2) can be rewritten as

$$\epsilon(R) = [84.32(\gamma - 1)]^{-1} U(R) T_0 R_0^\alpha R^{-\alpha-1} [3(\delta - 1) - \alpha]. \quad (4)$$

We assume that CMEs typically start out with a proton temperature $T_0 = 10^6 \text{ K}$ at $R_0 = 1.05 R_\odot$. *In situ* measurements give the CME speed U and proton temperature T near the Earth, using which we can calculate α from equation (3). Using equation (4), we can now estimate the ‘additional local’ power ϵ ($\text{J kg}^{-1} \text{s}^{-1}$) needed to heat the CME protons for a given value of the polytropic index δ . We would generally expect the power requirement to be higher for adiabatic evolution ($\delta \approx 5/3$), as compared to that for isothermal evolution ($\delta \approx 1$). This is because for isothermal expansion, the CME plasma expected to be thermally connected with an external reservoir such as the solar corona. One possibility could be efficient thermal conduction along large-scale magnetic fields connecting the CME with the corona. The additional local heat input needed to maintain the CME temperature is therefore expected to be negligible. On the other hand, for adiabatic expansion, the CME is expected to be thermally isolated from its surroundings. Therefore, there needs to be substantial additional local heat input in order to maintain the temperature. Similar treatments have been used to estimate the plasma heating rate in the solar wind (Livadiotis 2019).

3 POWER AVAILABLE IN TURBULENT VELOCITY FLUCTUATIONS

Having estimated the power requirement for proton heating, we turn our attention to the possible source(s). Turbulence in the solar wind is extensively studied (Bruno & Carbone 2013; Cranmer & Winebarger 2019) and the power in turbulent fluctuations is often invoked as the source for extended heating (Chandran & Hollweg 2009; Livadiotis 2019; Smith & Vasquez 2021; Shankarappa, Klein &

Martinović 2023). The interiors of CMEs are also similarly turbulent (Bhattacharjee et al. 2023; Shaikh 2024), and turbulent fluctuations are often invoked as a source of CME heating (Liu et al. 2006; Sorriso-Valvo et al. 2021). The cascade rate (ϵ_t) represents the power per unit mass contained in the inertial range of the turbulent velocity spectrum, and this is potentially available for proton heating at small scales such as the proton inertial length or the proton gyroradius (Liu et al. 2006; Sasikumar Raja et al. 2021). We use the well-known Kolmogorov turbulent cascade rate $\epsilon_t \propto \Delta U_k^3 k$ (e.g. chapter 6, Pope 2000), which relates the power per unit mass (ϵ_t) in the turbulent cascade to the fluid velocity fluctuations ΔU_k at scale k^{-1} . Using a dimensionless constant of proportionality C_0 , the Kolmogorov cascade rate becomes

$$\epsilon_t = C_0 k (\Delta U_k)^3 \text{ J kg}^{-1} \text{ s}^{-1}, \quad (5)$$

and we adopt $C_0 = 0.25$ following Howes et al. (2008) and Chandran et al. (2009). The quantity ΔU_k denotes the turbulent plasma velocity fluctuation at (spatial) wavenumber k , and is evaluated as the root-mean-square (rms) velocity fluctuation inside a moving box of temporal extent t_{box} . The wavenumber is expressed as $k \equiv 2\pi/(t_{\text{box}} U_{\text{MO}})$, where U_{MO} is the running average velocity of the magnetic obstacle (MO) inside the given t_{box} . The Magnetic Field Investigator (MFI) data we use has a time resolution of 1 min; however, when used with the Solar Wind Experiment (SWE) data, it provides a time resolution of ≈ 92 s. We take two values for t_{box} : 40 and 60 min, respectively. These values for t_{box} ensure that the wavenumbers are well within the expected inertial range. We note that the equation for ϵ_t used in Chandran et al. (2009) differs from ours by a factor of ρ (the plasma mass density), since their definition has units of $\text{J cm}^{-3} \text{ s}^{-1}$. The power available in the turbulent velocity spectrum (ϵ_t , equation 5) can be compared with the power required to heat the CME protons (ϵ , equation 4). Several studies (Liang et al. 2012; Li et al. 2016; Scolini et al. 2024) suggest that the inertial range turbulent spectrum in ICMEs is Alfvénic. Although Alfvénic fluctuations involve fluid velocity as well as magnetic field fluctuations, we have only considered the available power in the turbulent velocity fluctuations in writing equation (5), as Chandran et al. (2009) do, for instance. Strictly speaking, ΔU_k should denote the fluid velocity fluctuations perpendicular to the large-scale magnetic field, but we ignore this point for simplicity. For an Alfvénic spectrum (assuming Kolmogorov scaling), one could also consider the available power in the turbulent magnetic field fluctuations, $\Delta B_k^2/\mu_0\rho$, which is on the same footing as ΔU_k^2 (e.g. Leamon et al. 1999). For Alfvénic fluctuations, $\Delta U_k^2 = \Delta B_k^2/\mu_0\rho$. Since $\Delta U_k^3 = (\Delta U_k^2)^{3/2}$, it follows that adding the available power in turbulent magnetic fluctuations would mean replacing the quantity C_0 with $2^{3/2}C_0$.

4 DATA

For this study, we select a sample of well-observed near-Earth ICMEs detected by the WIND spacecraft (<https://wind.nasa.gov/>) during solar cycle 24 that resulted in geomagnetic storms with $D_{\text{st}} < -75$ nT. This yields a list of 27 events, which are listed in Table A1. The CMEs in solar cycle 24 are found to expand more than those in solar cycle 23, probably due to an overall (≈ 40 per cent) reduction of the total pressure in the heliosphere in solar cycle 24 (Gopalswamy et al. 2014). Although the overexpansion would dilute the stored magnetic energy in these CMEs (Gopalswamy et al. 2014), some of them still caused geomagnetic storms with D_{st} indices as high as -198 nT. This makes the geoeffective storms in cycle 24 an interesting data set to study. Table A1 also mentions the classification of the event based on its magnetic field profile

(Nieves-Chinchilla et al. 2016, 2018). Because of the diversity of the magnetic field configurations associated with ICMEs as observed using *in situ* spacecraft, Nieves-Chinchilla et al. (2018) introduced the term ‘magnetic obstacles’ or ‘MOs’. MOs are defined as plasma structures in closed magnetic loops embedded in ICMEs (Nieves-Chinchilla et al. 2018). The complex magnetic structures that do not follow the definition of magnetic clouds or flux rope configuration can also be considered as MOs. The MOs associated with the ICMEs are classified into different categories depending upon how well the observed magnetic field directions fit the expectations of a static flux rope configuration (Nieves-Chinchilla et al. 2016, 2018). Events indicate MOs with a single magnetic field rotation between 90° and 180° , F+ events indicate MOs with a single magnetic field rotation greater than 180° , and F− events indicate MOs with a single magnetic field rotation less than 90° . Events labelled ‘complex’ (Cx) have more than one magnetic field rotations, while the ‘ejectas’ (Ejs) do not have any particular rotation (Nieves-Chinchilla et al. 2019). For this study, we use the 1-min cadence data from the MFI (Lepping et al. 1995), which when measured with SWE (Ogilvie et al. 1995) data provide us with a time resolution of ≈ 92 s. These two instruments (MFI and SWE) are onboard the WIND spacecraft. The WIND ICME catalogue (wind.nasa.gov/ICMEindex.php) (Nieves-Chinchilla et al. 2018) provides the event details along with the start and end times for each of the MO listed in Table A1. The plasma velocity profile as a function of time inside the MO for each of these events is provided by the WIND/SWE instrument. We use the time series of the proton temperature from the OMNI data base (<https://omniweb.gsfc.nasa.gov/>) (King & Papitashvili 2005) considering the 1-min cadence data associated with the WIND plasma Key Parameters (KP). This is because the data from the MFI and SWE instruments (<https://wind.nasa.gov/mfi.swe.plot.php>) do not provide us with the time profile of proton temperature. We note that one can also derive temperature indirectly from the proton thermal speed (v_{th}) measured by the WIND/SWE. However, this method requires assumption on whether to use v_{th} as the mean, rms, or most probable speed of the distribution. We compute the magnitudes of velocity fluctuation inside the ICMEs following the method adopted by Bhattacharjee et al. (2023). The fluctuations are rms deviations around the mean inside a moving window of duration t_{box} . The spatial wavenumber corresponding to a value of t_{box} is $k = 2\pi/l$, where the length-scale for a given t_{box} is defined as $l = U_{\text{MO}} t_{\text{box}}$. U_{MO} is the running average of plasma velocity inside the MO for a given t_{box} (Bhattacharjee et al. 2023). The magnitude of the corresponding velocity fluctuation in the MO is ΔU_k . These are used in equation (5) to calculate the power in the turbulent velocity fluctuations. We use the terms ‘MO’ and ‘CME’ interchangeably, in the rest of the paper.

5 RESULTS

Fig. 1 shows a time series of ϵ_t (equation 5) for two representative events in our sample (Table A1) using $t_{\text{box}} = 40$ and 60 min (Bhattacharjee et al. 2023). We choose these two time boxes because they correspond to wavenumbers that are well within the inertial scale of the turbulent spectrum (Bhattacharjee et al. 2023), and are thus suitable to evaluate the turbulent energy cascade rate. Using $t_{\text{box}} = 40$ min yields ≈ 55 data points within the MO, while $t_{\text{box}} = 60$ min yield ≈ 40 data points. Similar plots for all the events are included in the supplementary material of this paper. Fig. 2 depicts histograms of $\langle \epsilon_t \rangle$ for the events listed in Table A1 using $t_{\text{box}} = 40$ and $t_{\text{box}} = 60$. The most probable value (mpv) is relevant for such skewed histograms. Since the mpv is somewhat sensitive to the

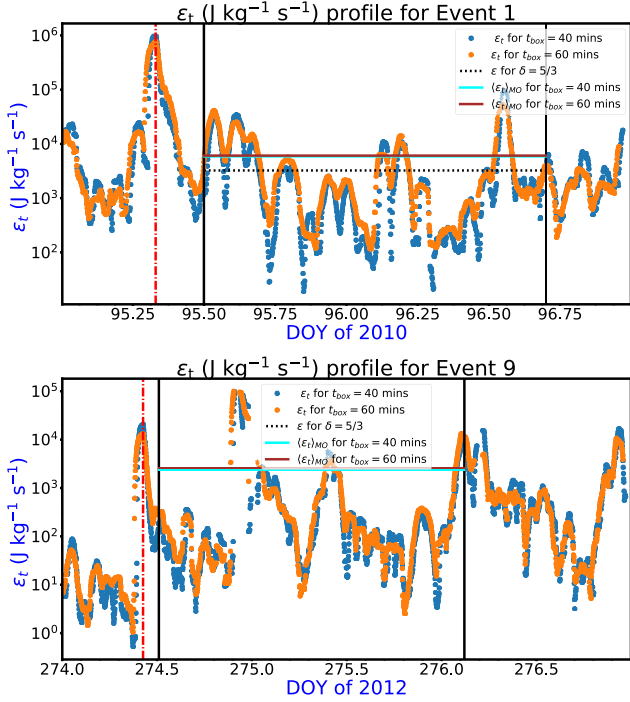


Figure 1. Time profiles of turbulent energy cascade rate (ϵ_t , equation 5) for event 1 (top panel) and event 9 (bottom panel) of the ICME list (Table A1). The blue and orange scatterplots represent ϵ_t using $t_{\text{box}} = 40$ and 60 min, respectively. The black vertical lines mark the MO boundaries and the red vertical line shows the ICME start (wind.nasa.gov/ICMEindex.php). The brown horizontal line inside represents the average ϵ_t using $t_{\text{box}} = 60$ min and the black dotted horizontal line represents the required power (ϵ , equation 4) using $\delta = 5/3$.

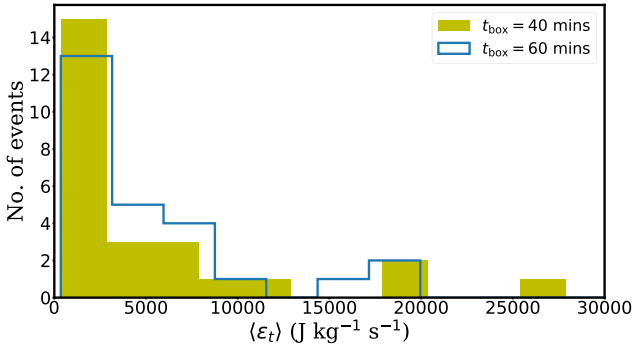


Figure 2. Histograms showing $\langle \epsilon_t \rangle$ for events listed in Table A1 using $t_{\text{box}} = 40$ min and $t_{\text{box}} = 60$ min respectively. The mean, median, and most probable value for $t_{\text{box}} = 40$ are 7646, 2674, and 1686 $\text{J kg}^{-1} \text{s}^{-1}$, respectively. The mean, median, and most probable value for $t_{\text{box}} = 60$ are 7750, 3486, and 1850 $\text{J kg}^{-1} \text{s}^{-1}$, respectively.

histogram bin size, we use the ‘auto’ option in matplotlib for bin size selection (following Ghuge, Bhattacharjee & Subramanian 2025), which chooses the smaller of the bin sizes recommended by the Sturges and Freedman-Diaconis methods. The mpv for the $t_{\text{box}} = 40$ histogram is 1686 $\text{J kg}^{-1} \text{s}^{-1}$ and that for the $t_{\text{box}} = 60$ histogram is 1850 $\text{J kg}^{-1} \text{s}^{-1}$. These numbers represent the (mpv of) power input to the protons. They may be compared with the power in the turbulent cascade that is potentially available for the dissipation on protons. Equation (5) represents a simple calculation of the turbulent

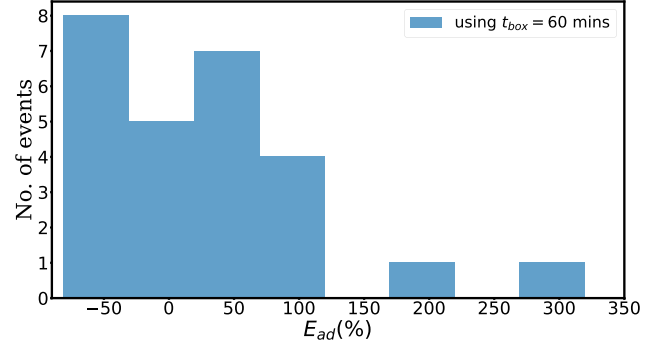


Figure 3. Histogram of E_{ad} (equation 6) for $t_{\text{box}} = 60$ min. The mean, median, and mpv are 53.25, 25.24, and -53.8 , respectively.

power, and representative results from this calculation are shown in Fig. 1. More detailed calculations of the available turbulent power in CMEs can be found, for instance, in Sorriso-Valvo et al. (2021).

Since the gross trends for ϵ_t are not very sensitive to the value of t_{box} , we use $t_{\text{box}} = 60$ min henceforth. The brown horizontal line in Fig. 1 denotes the average value of ϵ_t inside the MO (with $t_{\text{box}} = 60$ min), while the black horizontal line denotes the value of ϵ (equation 4) with $\delta = 5/3$ and $R = 215 R_{\odot}$. For the event depicted in the upper panel of Fig. 1, $\epsilon_t > \epsilon$, while $\epsilon_t \approx \epsilon$ for the event depicted in the lower panel.

Next, we compare the turbulent energy cascade rate (ϵ_t) estimated inside MOs with the required proton heating rate (ϵ) for $\delta = \gamma = 5/3$. This value for δ presumes adiabatic expansion and is commonly used in several studies, e.g. global 3D MHD simulations (Riley et al. 2003; Wu et al. 2016), studies of CME–CME interaction (Lugaz, Manchester IV & Gombosi 2005b), studies of CME expansion (Lugaz, Manchester IV & Gombosi 2005a), and many more. We define

$$E_{\text{ad}} \equiv 100 \frac{\epsilon_t - \epsilon}{\epsilon} \text{ per cent}, \quad (6)$$

which is the relative (percentage) difference between the power available in the turbulent velocity fluctuations (equation 5) and the power required for proton heating if they are assumed to remain adiabatic (equation 4 with $R = 215$ and $\delta = 5/3$). The histogram for E_{ad} for all the events in our sample using $t_{\text{box}} = 60$ min is shown in Fig. 3. The mpv of E_{ad} (which is the relevant quantity for a skewed distribution such as this one) is -54 per cent. In other words, Fig. 3 suggests that the power in the turbulent velocity fluctuations is ≈ 54 per cent lower than what is required to heat the protons if they are adiabatic. Needless to say, the value of E_{ad} will be quite different for other assumed values of δ , but $\delta = 5/3$ is a reasonable reference value considering how often it is used in the literature.

None the less, it is not (a priori) clear what value should be used for the polytropic index (δ) in a CME propagation model. The preceding discussion suggests that the adiabatic expansion for the protons could be too ‘demanding’, in that the energy in the turbulent velocity spectrum is not enough to provide the required local heating. On the other hand, the power required for local proton heating would be low if the protons were nearly isothermal. By way of estimating the ‘correct’ value for δ at a specific heliocentric distance and for a given wavenumber, we equate the power in the velocity fluctuations for a certain wavenumber (ϵ_t , equation 5) to the power required for proton heating (ϵ , equation 4) at that specific heliocentric distance. Using the estimates of ϵ_t and ϵ at the location of the WIND spacecraft

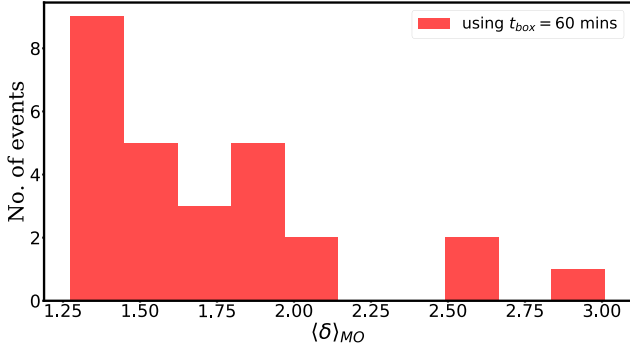


Figure 4. Histogram of estimated time-averaged polytropic index considering the turbulent energy cascade as the source of proton heating inside the near-Earth MOs ($\langle \delta \rangle_{MO}$, equation 7) for $t_{box} = 60$ min. The mean, median, and mpv of this histogram are 1.72, 1.59, and 1.35, respectively.

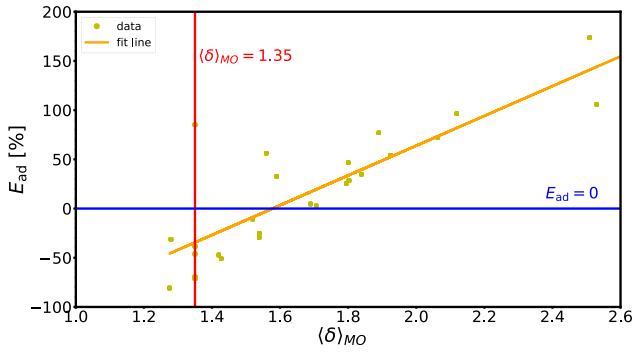


Figure 5. A scatterplot between $\langle \delta \rangle_{MO}$ (equation 7) and E_{ad} (equation 6) for the events in this study. The yellow line shows the best linear fit between these two parameters. The red vertical line is at $\langle \delta \rangle_{MO} = 1.35$, while the blue horizontal line denotes $E_{ad} = 0$.

(≈ 1 au or $R = 215R_{\odot}$), we can therefore compute the following:

$$\langle \delta \rangle_{MO} = \frac{1}{3} \left[\alpha + 3 + 84.32(\gamma - 1)(U(R) R_0^{\alpha} T_0)^{-1} R^{\alpha+1} \langle \epsilon_t \rangle \right], \quad (7)$$

where $\langle \epsilon_t \rangle$ denotes the time-averaged value ϵ_t inside an MO and $\langle \delta \rangle_{MO}$ the time-averaged value of the polytropic index inside the MO. The histogram of $\langle \delta \rangle_{MO}$ with $R = 215R_{\odot}$ and $t_{box} = 60$ min (Fig. 4) shows that it ranges from 1.25 to 3, with a mpv of 1.35. We have noted that ϵ generally exceeds ϵ_t with $\delta = 5/3$ (Fig. 3). It is therefore not surprising that the mpv of $\langle \delta \rangle_{MO}$ (which is obtained by equating ϵ with ϵ_t) is lower than $5/3$. Fig. 5 shows a scatterplot between $\langle \delta \rangle_{MO}$ and E_{ad} . The linear fit between $\langle \delta \rangle_{MO}$ and E_{ad} (depicted by the yellow line) has an intercept of -39.7 per cent at $\langle \delta \rangle_{MO} = 1.35$ (the red vertical line in Fig. 5). In other words, at $\langle \delta \rangle_{MO} = 1.35$, the power stored in the turbulent fluctuations is ≈ 40 per cent lower than the power required to heat the protons assuming adiabatic expansion. Equation (7) shows that $\langle \delta \rangle_{MO}$ depends on the initial temperature (T_0) we assume. In order to check the sensitivity of $\langle \delta \rangle_{MO}$ to T_0 , we compute it using three different initial temperatures: $T_0 = 10^6$ K, 1.5×10^6 K, and 2×10^6 K, respectively, and $t_{box} = 60$ min. The results are shown in the histograms of Fig. 6. The mpv of $\langle \delta \rangle_{MO}$ increases by ≈ 3 per cent upon doubling the initial temperature (i.e.

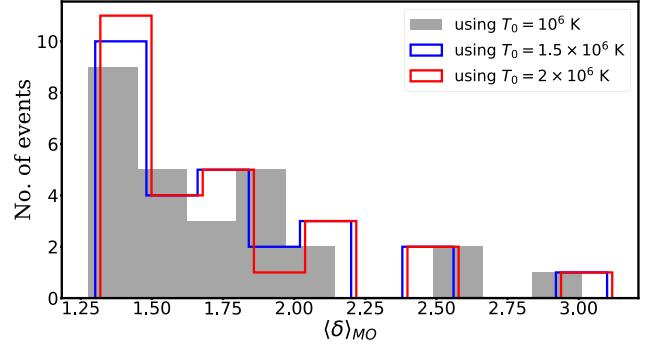


Figure 6. Same as Fig. 4, for different values of the initial temperature T_0 . For $T_0 = 10^6$ K the mean, median, and mpvs are 1.72, 1.59, and 1.35, respectively; for $T_0 = 1.5 \times 10^6$ K the mean, median, and mpvs are 1.74, 1.60, and 1.37, respectively; and for $T_0 = 2 \times 10^6$ K: the mean, median, and mpvs are 1.75, 1.61, and 1.39, respectively.

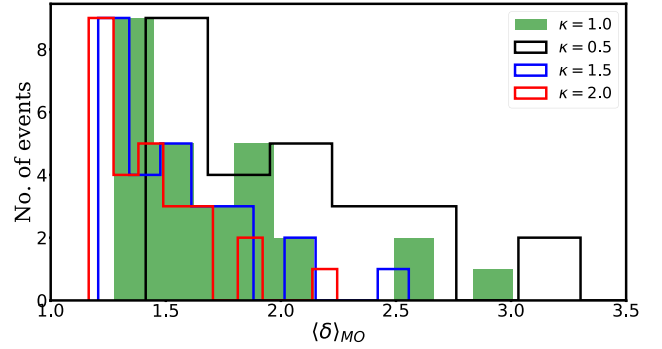


Figure 7. Histograms of $\langle \delta \rangle_{MO}$ for different values of κ . For $\kappa = 0.5$, the mean, median, and mpv of the histogram are 2.11, 2.03, and 1.52, respectively. For $\kappa = 1$ (self-similar evolution, where the CME minor radius $a \propto r$), they are 1.72, 1.59, and 1.35, respectively. For $\kappa = 1.5$, they are 1.56, 1.52, and 1.28, respectively. For $\kappa = 2$, they are 1.45, 1.41, and 1.23, respectively.

$T_0 = 2 \times 10^6$ K instead of 10^6 K). This implies that $\langle \delta \rangle_{MO}$ depends only weakly on the assumed initial temperature (T_0).

If the CME did not expand in a self-similar manner, i.e. if the minor radius (a) were to follow $a \propto r^{\kappa}$ (instead of $a \propto r$ as we have assumed, r being the radial distance of the CME from the Sun), the change in CME volume, dV/dr , would be $(2\kappa + 1)V/r$ instead of $3V/r$ and the number 3 in the second term on the right-hand side of equation (2) would be replaced with $2\kappa + 1$. The histograms in Fig. 7 show how $\langle \delta \rangle_{MO}$ varies with changes in κ . We adopt four different values for κ ($\kappa = 0.5, 1.0, 1.5$, and 2.0). We note that $\kappa = 1$ corresponds to self-similar expansion (i.e. $a \propto r$). For $\kappa = 2$, the mpv of $\langle \delta \rangle_{MO}$ is 8 per cent lower than that for $\kappa = 1$. For $\kappa = 1.5$, the mpv of $\langle \delta \rangle_{MO}$ is 5 per cent lower than that for $\kappa = 1$, while it is 13 per cent higher for $\kappa = 0.5$. Our findings therefore suggest that the polytropic index decreases with the cross-sectional expansion of the CMEs (see Fig. 7). If the volume evolution were more involved than a situation that can be accommodated by the $a \propto r^{\kappa}$ prescription, we would have to prescribe dV/dr accordingly in going from equation (A8) to equation (A9).

Equation (7) also shows that $\langle \delta \rangle_{MO}$ is approximately proportional to $\langle \epsilon_t \rangle$. This suggests that the closer $\langle \delta \rangle_{MO}$ is to its isothermal value of 1, the lower the requirement for local heating via turbulent dissipation. This is expected because, if the protons in the MO are close to isothermal, it implies that they are thermally well connected

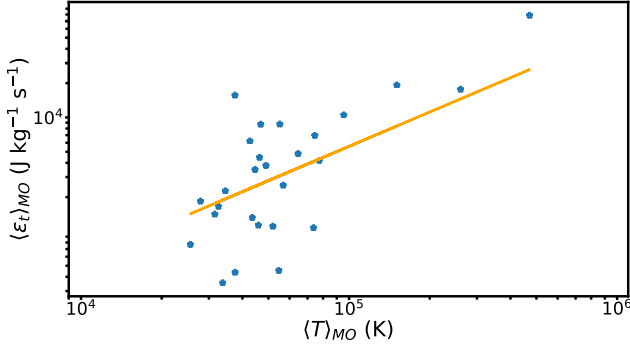


Figure 8. A scatterplot between the mean temperature ($\langle T \rangle_{\text{MO}}$) and average turbulent energy cascade rate ($\langle \epsilon_t \rangle_{\text{MO}}$) inside the MOs associated with the events listed in Table A1. The equation of the straight line fit is $y = 0.056x - 0.125$. The Pearson's correlation coefficient (r) is 0.93 with a p -value of 2.04×10^{-12} .

to an external heat reservoir (such as the solar corona). Good thermal 'connection' would imply a high thermal conductivity. Careful estimates of thermal conductivity in the turbulent collisionless solar wind plasma would be needed to justify this.

6 SUMMARY AND CONCLUSIONS

6.1 Summary

CMEs are observed to expand as they propagate through the heliosphere. Such expansion will be accompanied by plasma cooling, with heating/cooling processes being typically treated (implicitly) via a polytropic index (δ). If the expansion is adiabatic (δ close to $5/3$), the CME plasma temperature will be as low as a few tens of Kelvin when it reaches the Earth. Since observed proton temperatures in near-Earth CMEs are $\approx 10^5$ K, this calls for significant local heating as CMEs propagate. If, on the other hand, the CME plasma maintains significant thermal contact with the solar corona, it can be expected to be nearly isothermal ($\delta \approx 1$) and the local heating requirement is minimal. Since the CME magnetic fields are usually considered to be the basic energy reservoir, a higher demand on local heating translates to a lesser energy available for propagation, and vice versa. The value of δ adopted in a CME propagation model thus substantially affects the predictions of the Sun–Earth propagation time and the Earth arrival speed. In this paper, we obtain an expression relating the local heating rate (ϵ) corresponding to the polytropic index δ (equation 4). The quantity ϵ can be regarded as the local heating rate required by a model that uses a given polytropic index δ . On the other hand, the turbulent fluctuations in CMEs are often invoked as a plausible source of proton heating. Using observations of 27 well-observed geoeffective CMEs in solar cycle 24, we compute the power (ϵ_t) available in the turbulent velocity fluctuations (equation 5). The quantity ϵ_t can be thought of as the power that is potentially available to heat the CME plasma. Our main findings upon comparing ϵ with ϵ_t are as follows:

- (i) The available power (ϵ_t) is ≈ 54 per cent lower than the power (ϵ) required with $\delta = 5/3$ (Fig. 3).
- (ii) If, instead, the required power (ϵ) is taken to be equal to the available power (ϵ_t), the mpv for δ is 1.35 (Fig. 4).

Interestingly, we find a strong correlation between the average dissipation rate ($\langle \epsilon_t \rangle$) and the temperature ($\langle T \rangle$) in the CME (Fig. 8).

The Pearson correlation coefficient between $\langle \epsilon_t \rangle$ and $\langle T \rangle$ is 0.93, with a low p -value of 10^{-12} , which implies that the correlation is significant and reliable. We note that our results regarding the comparison of ϵ_t with ϵ and the estimate of $\langle \delta_{\text{MO}} \rangle$ are valid only near the Earth. In principle, equation (2) holds for any heliocentric distance R , provided the CME velocity U and temperature T is known. If the correlation between $\langle \epsilon_t \rangle$ and $\langle T \rangle$ generally holds true, it will allow us to estimate δ_{MO} for heliocentric distances between the Sun and the Earth, using reasonable models for $T(R)$ and $U(R)$.

6.2 Discussion

Estimates of CME arrival time and velocity (at the Earth) are vital inputs to space weather prediction. CME propagation models that calculate these quantities usually invoke CME magnetic fields and turbulent fluctuations as energy reservoirs. The polytropic index is often taken to be an adjustable parameter in such models. Our results show the relation between the polytropic index (δ), CME velocity (U), proton temperature (T), and the local energy dissipation rate (ϵ_t).

Assuming that the power in the turbulent velocity fluctuations partially provides for the work expended in CME expansion close to the Earth, we arrive at an estimate for the mpv of the polytropic index in near-Earth CMEs, $\langle \delta \rangle_{\text{MO}} = 1.35$. This can be taken to be a suggestion for the polytropic index to be adopted in CME propagation models. The most probable estimate of 1.35 is likely to be an upper limit for δ , for not all the power in the turbulent velocity fluctuation spectrum is likely to be expended in proton heating. Incidentally, Kumar & Rust (1996) obtain $\delta = 1.33$ by assuming that the energy input (dQ) to the CME is a fraction of the energy contained in the CME magnetic fields (without specifying the mechanism by which magnetic energy is converted into plasma heating).

We have so far used assumed values of $T_0 = 10^6$ K at $R = 1.05 R_\odot$ and observed values for the CME velocity (U), velocity fluctuations (ΔU_k), and proton temperature (T) to calculate α (equation 3), $\langle \epsilon_t \rangle$ (equation 5), and δ (equation 7). However, it is also worth examining some of the parametric dependencies from equation (7). These are as follows:

- (i) All else remaining fixed, the CME velocity increases with a decrease in δ . Specifically, using fiducial values of $T_0 = 10^6$ K, $R = 1.05 R_\odot$, and $\langle \epsilon_t \rangle = 10^4 \text{ J kg}^{-1} \text{ s}^{-1}$, equation (7) shows that decreasing δ from 1.38 to 1.3 (a decrease of 5 per cent) results in an increase in the CME velocity (at $R = 215 R_\odot$) from 250 to 500 km s^{-1} (an increase of 100 per cent). This confirms what CME modellers recognize; assuming a thermodynamic equation of state that is close(r) to isothermal generally results in faster CMEs. These findings are also in agreement with those of Khuntia et al. (2024).

- (ii) All else remaining fixed, a decrease in δ results in a decrease in α (equation 3), which means that the proton temperature decreases slower with heliocentric distance. Using fiducial values of $T_0 = 10^6$ K, $R = 1.05 R_\odot$, $\langle \epsilon_t \rangle = 10^4 \text{ J kg}^{-1} \text{ s}^{-1}$, and a CME velocity of 400 km s^{-1} at $R = 215 R_\odot$, equation (7) shows that decreasing δ from 1.38 to 1.3 (a decrease of 5 per cent) results in α decreasing from 0.85 to 0.6 (a decrease of 29 per cent). In other words, the rate of decrease of the proton temperature (with heliocentric distance) is slower. This will be manifested as a relatively higher proton temperature at the Earth. This trend is borne out by solar wind simulations (e.g. Mayank, Vaidya & Chakrabarty 2022) where the predicted proton

temperature at the Earth is higher for polytropic indices that are closer to 1.

(iii) As mentioned in the discussion following equation (5) in Section 3, including the power potentially available in magnetic fluctuations (in addition to the power potentially available in velocity fluctuations) results in the quantity C_0 being replaced by $2^{3/2}C_0$. Using $\langle \epsilon_t \rangle = 2^{3/2} \times 10^4 \text{ J kg}^{-1} \text{ s}^{-1}$, and a CME velocity of 400 km s^{-1} at $R = 215 R_\odot$ in equation (7) gives $\delta = 1.45$ (which can be regarded as an increase of ≈ 7.4 per cent over the mpv of $\delta = 1.35$, which was obtained without the factor of $2^{3/2}$).

(iv) An alternative approach to the one we have taken in this paper would be to observationally determine the polytropic index in MOs and their sheaths using fits to a $T \propto n^{\delta-1}$ scatterplot (e.g. Katsavrias et al. 2025). Equation (7) could then be used to compute the power that needs to be dissipated on the protons, as implied by this value of the polytropic index.

ACKNOWLEDGEMENTS

The authors thank the Indo-US Science and Technology Forum (IUSSTF) for supporting the current project. DB acknowledges the support from the University of Glasgow to meet the Open Access Publication of this paper. This paper has benefitted from helpful inputs from the anonymous reviewer.

DATA AVAILABILITY

The main data used in this article are available on the WIND website (<https://wind.nasa.gov/>). The data detailing the event list and estimated parameters are available in this article and can be used with proper citations.

REFERENCES

Akmal A., Raymond J. C., Vourlidis A., Thompson B., Ciaravella A., Ko Y. K., Uzzo M., Wu R., 2001, *ApJ*, 553, 922
 Balmaceda L. A., Vourlidis A., Stenborg G., St. Cyr O. C., 2020, *Sol. Phys.*, 295, 107
 Bhattacharjee D., Subramanian P., Nieves-Chinchilla T., Vourlidis A., 2023, *MNRAS*, 518, 1185
 Bruno R., Carbone V., 2013, *Living Rev. Sol. Phys.*, 10, 2
 Chandran B. D. G., Hollweg J. V., 2009, *ApJ*, 707, 1659
 Chandran B. D. G., Quataert E., Howes G. G., Xia Q., Pongkitiwanichakul P., 2009, *ApJ*, 707, 1668
 Chen J., 1996, *J. Geophys. Res.*, 101, 27499
 Ciaravella A., Raymond J. C., Reale F., Strachan L., Peres G., 2001, *ApJ*, 557, 351
 Cranmer S. R., Winebarger A. R., 2019, *ARA&A*, 57, 157
 Davies J. A. et al., 2012, *ApJ*, 750, 23
 Dayeh M. A., Livadiotis G., 2022, *ApJ*, 941, L26
 Démoulin P., 2009, *Sol. Phys.*, 257, 169
 Farrugia C. J., Osherovich V., Burlaga L., 1995, *J. Geophys. Res.*, 100, 12293
 Ghuge D., Bhattacharjee D., Subramanian P., 2025, *Sol. Phys.*, 300, 47
 Gopalswamy N., Lara A., Yashiro S., Kaiser M. L., Howard R. A., 2001, *J. Geophys. Res.*, 106, 29207
 Gopalswamy N., Akiyama S., Yashiro S., Xie H., Mäkelä P., Michalek G., 2014, *Geophys. Res. Lett.*, 41, 2673
 Howes G. G., Cowley S. C., Dorland W., Hammett G. W., Quataert E., Schekochihin A. A., 2008, *J. Geophys. Res.*, 113, A05103
 Katsavrias C., Nicolaou G., Livadiotis G., Vourlidis A., Wilson III L. B., Sandberg I., 2025, *A&A*, 695, 11
 Khuntia S., Mishra W., Mishra S. K., Wang Y., Zhang J., Lyu S., 2023, *ApJ*, 958, 92

Khuntia S., Mishra W., Wang Y., Mishra S. K., Nieves-Chinchilla T., Lyu S., 2024, *MNRAS*, 535, 2585
 King J. H., Papitashvili N. E., 2005, *J. Geophys. Res.: Space Phys.*, 110, A02104
 Kumar A., Rust D. M., 1996, *J. Geophys. Res.*, 101, 15667
 Leamon R. J., Smith C. W., Ness N. F., Wong H. K., 1999, *J. Geophys. Res.*, 104, 22331
 Lee J. Y., Raymond J. C., Ko Y. K., Kim K. S., 2009, *ApJ*, 692, 1271
 Lepping R. et al., 1995, *Space Sci. Rev.*, 71, 207
 Li H., Wang C., He J., Zhang L., Richardson J. D., Belcher J. W., Tu C., 2016, *ApJ*, 831, L13
 Liang H., Xiao C., Zhou G., Pu Z., Wang H., Wang X., 2012, *Plasma Sci. Technol.*, 14, 102
 Lionello R., Downs C., Linker J. A., Török T., Riley P., Mikić Z., 2013, *ApJ*, 777, 76
 Liu Y., Richardson J., Belcher J., 2005, *Planet. Space Sci.*, 53, 3
 Liu Y., Richardson J. D., Belcher J. W., Kasper J. C., Elliott H. A., 2006, *J. Geophys. Res.*, 111, A01102
 Livadiotis G., 2019, *Entropy*, 21, 1041
 Lugaz N., Manchester IV W. B., Gombosi T. I., 2005a, *ApJ*, 627, 1019
 Lugaz N., Manchester IV W. B., Gombosi T. I., 2005b, *ApJ*, 634, 651
 Mandrini C. H., 2010, in Kosovichev A. G., Andrei A. H., Rozelot J.-P. eds, IAU Symp. 264, Solar and Stellar Variability: Impact on Earth and Planets. Cambridge Univ. Press, Cambridge, p. 257
 Mayank P., Vaidya B., Chakrabarty D., 2022, *ApJS*, 262, 23
 Mishra W., Wang Y., 2018, *ApJ*, 865, 50
 Möstl C., Davies J. A., 2013, *Sol. Phys.*, 285, 411
 Murphy N. A., Raymond J. C., Korreck K. E., 2011, *ApJ*, 735, 17
 Nicolaou G., Livadiotis G., Wicks R. T., Verscharen D., Maruca B. A., 2020, *ApJ*, 901, 26
 Nieves-Chinchilla T., Linton M. G., Hidalgo M. A., Vourlidis A., Savani N. P., Szabo A., Farrugia C., Yu W., 2016, *ApJ*, 823, 27
 Nieves-Chinchilla T., Vourlidis A., Raymond J. C., Linton M. G., Al-haddad N., Savani N. P., Szabo A., Hidalgo M. A., 2018, *Sol. Phys.*, 293, 25
 Nieves-Chinchilla T., Jian L. K., Balmaceda L., Vourlidis A., dos Santos L. F. G., Szabo A., 2019, *Sol. Phys.*, 294, 89
 Odstrčil D., 2023, *Front. Astron. Space Sci.*, 10, 1226992
 Odstrčil D., Pizzo V., 1999, *J. Geophys. Res.*, 104, 483
 Ogilvie K. et al., 1995, *Space Sci. Rev.*, 71, 55
 Osherovich V. A., Farrugia C. J., Burlaga L. F., Lepping R. P., Fainberg J., Stone R. G., 1993, *J. Geophys. Res.*, 98, 15331
 Pomoell J., Poedts S., 2018, *J. Space Weather Space Clim.*, 8, A35
 Pope S. B., 2000, Turbulent Flows. Cambridge Univ. Press, Cambridge
 Riley P., Linker J., Mikić Z., Odstrčil D., Zurbuchen T., Lario D., Lepping R. P., 2003, *J. Geophys. Res.*, 108, 1272
 Riley P. et al., 2018, *Space Weather*, 16, 1245
 Sasikumar Raja K., Subramanian P., Ingale M., Ramesh R., Maksimovic M., 2021, *ApJ*, 914, 137
 Scolini C., Lugaz N., Winslow R. M., Farrugia C. J., Magyar N., Bacchini F., 2024, *ApJ*, 961, 135
 Shaikh Z. I., 2024, *MNRAS*, 530, 3005
 Shankarappa N., Klein K. G., Martinović M. M., 2023, *ApJ*, 946, 85
 Smith C. W., Vasquez B. J., 2021, *Front. Astron. Space Sci.*, 7, 114
 Sorriso-Valvo L., Yordanova E., Dimmock A. P., Telloni D., 2021, *ApJ*, 919, L30
 Subramanian P., Arunbabu K. P., Vourlidis A., Mauriya A., 2014, *ApJ*, 790, 125
 Thernisien A., 2011, *ApJS*, 194, 33
 Totten T. L., Freeman J. W., Arya S., 1995, *J. Geophys. Res.*, 100, 13
 Vasquez B. J., Smith C. W., Hamilton K., MacBride B. T., Leamon R. J., 2007, *J. Geophys. Res.*, 112, A07101
 Verma M. K., Roberts D. A., Goldstein M. L., 1995, *J. Geophys. Res.*, 100, 19839
 Wang Y., Zhang J., Shen C., 2009, *J. Geophys. Res.*, 114, A10104
 Wu C.-C., Liou K., Vourlidis A., Plunkett S., Dryer M., Wu S., Mewaldt R. A., 2016, *J. Geophys. Res.*, 121, 56

SUPPORTING INFORMATION

Supplementary data are available at [MNRAS](https://mnras.oxfordjournals.org/) online.

epsilon-plots.new

Please note: Oxford University Press is not responsible for the content or functionality of any supporting materials supplied by the authors. Any queries (other than missing material) should be directed to the corresponding author for the article.

APPENDIX A: APPENDIX

A1 Relating the proton polytropic index to the local heating rate

We modify the treatment of Verma, Roberts & Goldstein (1995) and Vasquez et al. (2007) to obtain an equation for the evolution of proton temperature in a CME by accounting for a polytropic equation of state. As in Verma et al. (1995), we start with the energy conservation equation

$$dQ = dU' + PdV, \quad (\text{A1})$$

where dQ is the change in energy added to (or taken from) the CME, dU' is the change in internal energy, PdV is the work done in expanding/contracting the CME volume. The change in internal energy can be written as

$$dU' = NC_v dT, \quad (\text{A2})$$

where V and N are the volume of the CME and the number of moles contained in it, dT is the change in temperature and C_v is the specific heat at constant volume. Introducing $K \equiv dQ/PdV$ and using equation (A2), equation (A1) can be rewritten as

$$(K - 1)PdV = dU' = NC_v dT. \quad (\text{A3})$$

We introduce the polytropic law

$$PV^\delta = C \quad (\text{A4})$$

and differentiate it to get

$$\frac{dP}{P} + \delta \frac{dV}{V} = 0. \quad (\text{A5})$$

Similarly, differentiating the ideal gas law $PV = NRT$ (where $R \equiv C_p - C_v$) and using equation (A3) gives

$$[1 - (\gamma - 1)(K - 1)] \frac{dV}{V} + \frac{dP}{P} = 0, \quad (\text{A6})$$

where $\gamma \equiv C_p/C_v$ is the usual adiabatic index. Comparing equation (A6) and equation (A5) gives

$$K \equiv \frac{dQ}{PdV} = \frac{\delta - \gamma}{1 - \gamma}. \quad (\text{A7})$$

The energy conservation equation (equation A1) does not include ‘external’ contributions from sources such as turbulent dissipation. Accounting for such contributions and using equations (A2) and (A7), the energy conservation equation becomes

$$M\epsilon dt = dU' + PdV - dQ = NC_v dT + PdV \frac{1 - \delta}{1 - \gamma} \quad (\text{A8})$$

The quantity M represents the CME mass, dt the time elapsed, and ϵ ($\text{erg g}^{-1} \text{s}^{-1}$) the time rate per unit mass of additional energy deposition. The additional energy deposition term $M\epsilon dt$ is not accounted for in the original energy conservation equation (equation A1). It is ‘additional’ in the sense that it represents heating due to additional sources such as small-scale reconnection events inside the CME plasma, or from dissipation of turbulent fluctuations. We next differentiate equation (A8) with respect to r and write $dr/dt \equiv U(r)$, so that $U(r)$ represents the CME velocity. If the CME flux rope is idealized as a curved cylinder of cross-sectional radius a and length $\propto r$, its volume $V \propto a^2 r$. Since most CMEs expand in a self-similar manner with $a \propto r$, it follows that $V \propto r^3$, which means that $dV/dr = 3V/r$. This yields

$$\frac{M}{NC_v} \frac{\epsilon}{U} = \frac{dT}{dr} + 3 \frac{1 - \delta}{1 - \gamma} \frac{P}{NC_v} \frac{V}{r}. \quad (\text{A9})$$

Using the ideal gas law ($PV = NRT$), $R \equiv C_p - C_v$, and $M/(NC_v) = (\gamma - 1)m_p/k_B$ (m_p is the proton mass and k_B is the Boltzmann constant) in equation (A9), we get

$$\frac{dT(R)}{dR} = 84.32(\gamma - 1) \frac{\epsilon(R)}{U(R)} - 3(\delta - 1) \frac{T(R)}{R}, \quad (\text{A10})$$

where $R = r/R_\odot$ and $U(R)$ is the CME velocity in units of km s^{-1} . If we use $\delta = \gamma = 5/3$ and 2 in place of 3 in the second term on the right-hand side, equation (A10) is identical to equation (9) of Vasquez et al. (2007).

A2 Relevant tables

This section contains two tables. Table A1 gives details of the 27 events that are used in this paper. Table A2 lists ϵ (equation 4), $\langle \epsilon_t \rangle_{MO}$ (equation 5), $\langle \delta \rangle_{MO}$ (equation 7), and E_{ad} (equation 6) for all the events listed in Table A1.

Table A1. The list of the near-Earth ICME events we use in this study. The arrival date and time of the ICME at the position of the WIND measurement and the arrival and departure dates and times of the associated magnetic clouds (MOs) are taken from the WIND ICME catalogue (wind.nasa.gov/ICMEindex.php). The time between the ‘ICME start time’ and ‘MO start time’ is taken as the sheath duration.

ICME event number	ICME start date and time[UT] (1 au)	MO start date and time [UT]	MO end date and time [UT]	Flux rope type	D_{st} index (nT)
1	2010-04-05, 07:55	2010-04-05, 11:59	2010-04-06, 16:48	Fr	−81
2	2010-05-28, 01:55	2010-05-28, 19:12	2010-05-29, 17:58	Fr	−80
3	2011-05-28, 00:14	2011-05-28, 05:31	2011-05-28, 22:47	F+	−80
4	2011-10-24, 17:41	2011-10-25, 00:21	2011-10-25, 23:31	Cx	−147
5	2012-03-08, 10:32	2012-03-08, 19:55	2012-03-11, 07:26	Cx	−145
6	2012-06-16, 09:03	2012-06-16, 22:01	2012-06-17, 11:23	F+	−86
7	2012-07-08, 02:10	2012-07-08, 07:58	2012-07-10, 01:41	Cx	−78
8	2012-07-14, 17:39	2012-07-15, 06:14	2012-07-17, 03:21	Fr	−139
9	2012-09-30, 10:14	2012-09-30, 12:14	2012-10-02, 02:53	Cx	−122
10	2012-10-08, 04:12	2012-10-08, 15:50	2012-10-09, 17:17	Fr	−107
11	2012-10-12, 08:09	2012-10-12, 18:29	2012-10-13, 09:14	Fr	−90
12	2012-11-12, 22:12	2012-11-13, 08:23	2012-11-14, 08:09	F+	−108
13	2013-03-17, 05:21	2013-03-17, 14:09	2013-03-19, 16:04	Fr	−132
14	2013-03-06, 02:09	2013-06-06, 14:23	2013-06-08, 00:00	F+	−78
15	2013-06-27, 13:51	2013-06-28, 02:23	2013-06-29, 11:59	Fr	−102
16	2013-07-04, 17:17	2013-07-05, 04:05	2013-07-07, 14:24	Cx	−87
17	2014-09-12, 15:17	2014-09-12, 21:22	2014-09-14, 11:38	F−	−88
18	2015-01-07, 05:38	2015-01-07, 06:28	2015-01-07, 21:07	F+	−99
19	2015-06-22, 18:07	2015-06-23, 02:23	2015-06-24, 13:03	Cx	−198
20	2015-11-06, 17:46	2015-11-07, 07:11	2015-11-08, 16:47	Fr	−79
21	2015-12-19, 15:35	2015-12-20, 13:40	2015-12-21, 23:02	Fr	−155
22	2016-01-19, 03:31	2016-01-19, 11:23	2016-01-20, 14:19	Fr	−93
23	2016-10-12, 21:37	2016-10-13, 06:27	2016-10-14, 16:19	F+	−110
24	2017-05-27, 13:45	2017-05-27, 22:50	2017-05-29, 11:05	F+	−125
25	2017-09-06, 22:21	2017-09-07, 09:13	2017-09-08, 06:35	Ej	−122
26	2017-09-07, 16:17	2017-09-08, 00:19	2017-09-09, 16:57	Ej	−109
27	2018-08-25, 01:02	2018-08-25, 12:04	2018-08-25, 12:19	F+	−175

Table A2. The first column is the serial number of the event, taken from Table A1. The second column is the average proton temperature inside the MO. The third column is the required power (ϵ) using equation (4). The fourth column is the average turbulent cascade rate ($\langle\epsilon_t\rangle_{MO}$). The fifth column is the average polytropic index ($\langle\delta\rangle_{MO}$) obtained from equation (7). The sixth column is the percentage difference between ϵ and $\langle\epsilon_t\rangle_{MO}$ using equation (6).

ICME event number	Average proton temperature in MO (K)	ϵ (J kg ⁻¹ s ⁻¹)	$\langle\epsilon_t\rangle_{MO}$ $t_{\text{box}} = 60$ min (J kg ⁻¹ s ⁻¹)	$\langle\delta\rangle_{MO}$ $t_{\text{box}} = 60$ min (at 1 au)	E_{ad} (per cent) $t_{\text{box}} = 60$ min (at 1 au)
1	42661.07	3154.98	6198.88	2.12	96.48
2	37577.24	1522.35	437.40	1.35	-71.27
3	44599.27	2712.16	3486.56	1.80	28.55
4	95528.45	6100.42	10501.63	2.06	72.15
5	77455.27	5599.40	4188.05	1.54	-25.21
6	64545.57	3562.04	4802.49	1.84	34.82
7	32580.03	1523.78	1656.03	1.71	8.68
8	48978.26	2852.42	3614.58	1.59	32.66
9	56799.44	2427.59	2540.65	1.61	-19.13
10	46820.43	2252.08	8700.73	3.01	286.23
11	55167.73	3189.94	8729.32	2.51	173.65
12	73696.42	3509.89	1075.31	1.35	-69.63
13	46340.17	2885.91	4453.36	1.92	54.32
14	33756.76	1629.67	353.49	1.35	-78.39
15	25589.45	1086.06	767.25	1.54	-29.38
16	27901.36	1040.41	1840.02	1.89	76.86
17	74488.79	5546.86	6947.34	1.76	25.25
18	31567.11	1589.26	1246.12	1.57	-19.12
19	150787.24	12288.69	9877.82	1.56	56.32
20	43552.77	2692.16	1320.31	1.43	-50.96
21	45858.42	2148.55	1133.49	1.42	-47.24
22	37522.46	1556.93	4473.13	2.53	105.96
23	34547.13	1544.09	2265.36	1.80	46.72
24	54687.12	2360.98	453.71	1.28	-80.78
25	471530.44	42419.50	21387.22	1.35	85.28
26	260728.26	25678.55	8641.99	1.28	-31.36
27	51986.37	2527.93	1108.91	1.35	-46.14

This paper has been typeset from a \LaTeX file prepared by the author.